CHALMERS
FINITE ELEMENT CENTER

PREPRINT 2002–18

Adaptive strategies and error control for computing material forces in fracture mechanics

Per Heintz, Fredrik Larsson, Peter Hansbo, Kenneth Runesson

Chalmers Finite Element Center
CHALMERS UNIVERSITY OF TECHNOLOGY
Göteborg Sweden 2002

CHALMERS FINITE ELEMENT CENTER

Preprint 2002–18

Adaptive strategies and error control for computing material forces in fracture mechanics

Per Heintz, Fredrik Larsson, Peter Hansbo, Kenneth Runesson

CHALMERS

Chalmers Finite Element Center
Chalmers University of Technology
SE–412 96 Göteborg Sweden
Göteborg, December 2002

Adaptive strategies and error control for computing material forces in fracture mechanics
Per Heintz, Fredrik Larsson, Peter Hansbo, Kenneth Runesson
NO 2002–18
ISSN 1404–4382

Chalmers Finite Element Center
Chalmers University of Technology
SE–412 96 Göteborg
Sweden
Telephone: +46 (0)31 772 1000
Fax: +46 (0)31 772 3595
www.phi.chalmers.se

Printed in Sweden
Chalmers University of Technology
Göteborg, Sweden 2002

ADAPTIVE STRATEGIES AND ERROR CONTROL FOR COMPUTING MATERIAL FORCES IN FRACTURE MECHANICS

PER HEINTZ, FREDRIK LARSSON, PETER HANSBO, AND KENNETH RUNESSON

Abstract. The concept of material forces pertains to a variation of the inverse motion map while the placement field is kept fixed. From the weak formulation of the self-equilibrating Eshelby (material) stress tensor it turns out that the classical J-integral formulations in fracture mechanics are just special cases due to the choice of particular weight functions. In this contribution, we discuss a posteriori error control of the material forces as part of an adaptive strategy to reduce the discretization error to an acceptable level. The data of the dual problem involves the quite non-conventional tangent stiffness of the (material) Eshelby stress tensor with respect to a variation of the (physical) strain field. The suggested strategy is applied to the common fracture mechanics problem of a single-edged crack, whereby different strategies for computing the J-integral are compared. We also consider the case in which the crack edges are not parallel, i.e a notch.

1. Introduction

In this paper we discuss a goal-oriented error control algorithm for computing material forces in fracture mechanics. For an in-depth discussion of the theoretical background and the design of the algorithm for computing the material forces from the finite element solution, we refer to Steinmann et al. [1],[2]

The considered goal-quantities are derived from an equilibrium assumption and their corresponding linearization are presented as part of the data to the dual problem. We make a comparison between the different methods and present some numerical results. We also consider the case where the crack edges are not parallel so that the contribution from the edges can not be neglected.

The outline of the paper is as follows: In section 2 we recall the mathematical framework behind the adaptive strategy. In section 3, we give a brief introduction to the concept of material forces and its relation to the classical J-integral formulations in fracture mechanics. In section 4, we discuss some aspects on the chosen goal functionals and their linearization. Finally, in section 5 we consider the model problem of a single edge crack/notch in a linear elastic plate, whereby we present some adaptive results together with some conclusions.

Date: December 20, 2002.

Key words and phrases. Adaptivity, Error Control, Fracture mechanics, Material forces.

Per Heintz, Department of Applied Mechanics, Chalmers University of Technology, S–412 96 Göteborg, Sweden, *email*: per.heintz@me.chalmers.se.

2. Error Control based on a Dual Solution

We give a short review of the theoretical background and refer to [3], [4] and [5] for more in-depth discussions. See also [6] for work on goal-oriented a posteriori error estimates in elastic fracture mechanics.

The weak form of the primal problem is described with its semi-linear and linear forms

$$\text{Find } \boldsymbol{u} \in V: \quad a(\boldsymbol{u};\boldsymbol{v}) = F(\boldsymbol{v}) \qquad \forall \boldsymbol{v} \in V. \tag{2.1}$$

The FE approximation yields $\boldsymbol{u}_h \in V_h$ and we are interested in the error in a particular quantity. We denote the exact quantity by $Q(\boldsymbol{u})$ and introduce $E(\boldsymbol{u},\boldsymbol{u}_h)$ that measures the difference between the exact and the approximated quantity

$$E(\boldsymbol{u},\boldsymbol{u}_h) = Q(\boldsymbol{u}) - Q(\boldsymbol{u}_h). \tag{2.2}$$

The directional derivative for $E(\boldsymbol{u},\boldsymbol{u}_h)$ in the direction $\boldsymbol{w}$ is defined as

$$E'(\boldsymbol{u},\boldsymbol{u}_h;\boldsymbol{w}) = \frac{\partial}{\partial \epsilon} E(\boldsymbol{u}+\epsilon\boldsymbol{w},\boldsymbol{u}_{\boldsymbol{h}})|_{\epsilon=0}, \tag{2.3}$$

and the secant form of $E(\boldsymbol{u},\boldsymbol{u}_h)$ is obtained as

$$E_S(\boldsymbol{u},\boldsymbol{u}_h;\boldsymbol{w}) \;=\; \int_0^1 E'(\bar{\boldsymbol{u}}(s),\boldsymbol{u}_h;\boldsymbol{w})\mathrm{d}s, \tag{2.4}$$

where $\bar{\boldsymbol{u}}(s) = \boldsymbol{u}_h + s\boldsymbol{e}$. Choosing $\boldsymbol{w} = \boldsymbol{e} := \boldsymbol{u} - \boldsymbol{u}_h$ leads to

$$E_S(\boldsymbol{u},\boldsymbol{u}_h;\boldsymbol{e}) = E(\boldsymbol{u},\boldsymbol{u}_h) - E(\boldsymbol{u}_h,\boldsymbol{u}_h) = E(\boldsymbol{u},\boldsymbol{u}_h). \tag{2.5}$$

The dual bilinear form $a_S^*(\boldsymbol{u},\boldsymbol{u}_h;\boldsymbol{w},\boldsymbol{v})$ is defined as

$$a_S^*(\boldsymbol{u},\boldsymbol{u}_h;\boldsymbol{w},\boldsymbol{v}) = a_S(\boldsymbol{u},\boldsymbol{u}_h;\boldsymbol{v},\boldsymbol{w}) = \int_0^1 a'(\bar{\boldsymbol{u}}(s),\boldsymbol{v};\boldsymbol{w})\mathrm{d}s, \tag{2.6}$$

where $a_S(\boldsymbol{u},\boldsymbol{u}_h;\boldsymbol{v},\boldsymbol{w})$ is the secant stiffness of the primal problem. The abstract variational format of the dual problem is now defined as

$$\text{Find } \boldsymbol{\varphi} \in V: \quad a_S^*(\boldsymbol{u},\boldsymbol{u}_h;\boldsymbol{\varphi},\boldsymbol{v}) = E_S(\boldsymbol{u},\boldsymbol{u}_h;\boldsymbol{v}) \qquad \forall \boldsymbol{v} \in V. \tag{2.7}$$

Using the above definitions, the following exact error representation holds with $\boldsymbol{v} = \boldsymbol{e}$

$$\begin{aligned} E_S(\boldsymbol{u},\boldsymbol{u}_h;\boldsymbol{e}) &= a_S^*(\boldsymbol{u},\boldsymbol{u}_h;\boldsymbol{\varphi},\boldsymbol{e}) = a_S(\boldsymbol{u},\boldsymbol{u}_h;\boldsymbol{e},\boldsymbol{\varphi}) \\ &= a_S(\boldsymbol{u},\boldsymbol{u}_h;\boldsymbol{e},\boldsymbol{\varphi}-\pi_h\boldsymbol{\varphi}) \\ &= F(\boldsymbol{\varphi}-\pi_h\boldsymbol{\varphi}) - a(\boldsymbol{u}_h;\boldsymbol{\varphi}-\pi_h\boldsymbol{\varphi}). \end{aligned} \tag{2.8}$$

The third equality is obtained using the Galerkin orthogonality. In an adaptive scheme, the error representation formula is evaluated numerically on the element level, and elements with large contribution to the total error are chosen to be refined to the next grid-level.
Remark: When the primal problem is linear and symmetrical we have

$$a_S^*(\boldsymbol{u},\boldsymbol{u}_h;\boldsymbol{\varphi},\boldsymbol{v}) = a(\boldsymbol{\varphi},\boldsymbol{v}). \quad \square \tag{2.9}$$

3. Material forces and the J-integral in fracture mechanics

3.1. **Preliminaries.** Subsequently, we consider the case of small strains and quasi-static loading conditions. In absence of physical volume forces the physical (Cauchy) stress $\boldsymbol{\sigma}$ fulfills the quasi-static equilibrium equation

$$\nabla \cdot \boldsymbol{\sigma}^{\mathrm{T}} = \mathbf{0} \qquad \text{in } \Omega. \tag{3.1}$$

Similarly, in the absence of material volume forces, the material (Newton-Eshelby) stress $\tilde{\boldsymbol{\Sigma}}$ is also self-equilibrating

$$\nabla \cdot \tilde{\boldsymbol{\Sigma}}^{\mathrm{T}} = \mathbf{0} \qquad \text{in } \Omega. \tag{3.2}$$

The Newton-Eshelby stress is defined as

$$\tilde{\boldsymbol{\Sigma}} \stackrel{\text{def}}{=} W\boldsymbol{I} - \boldsymbol{H}^{\mathrm{T}} \cdot \boldsymbol{\sigma}, \tag{3.3}$$

where we used the notation $\boldsymbol{H}(\boldsymbol{u}) = \boldsymbol{u} \otimes \nabla$ and W is the strain energy density. The definition of $\tilde{\boldsymbol{\Sigma}}$ in (3.3) is commonly adopted as the generic material stress tensor in the mechanics of fracture and defects. Restricting the present discussion to linear elastic response, we have

$$W(\boldsymbol{u}) = \frac{1}{2}\boldsymbol{\epsilon}(\boldsymbol{u}) : \mathsf{E}^{\mathrm{e}} : \boldsymbol{\epsilon}(\boldsymbol{u}) = \frac{1}{2}\boldsymbol{H}(\boldsymbol{u}) : \mathsf{E}^{\mathrm{e}} : \boldsymbol{H}(\boldsymbol{u}), \tag{3.4}$$

$$\boldsymbol{\sigma}(\boldsymbol{u}) = \mathsf{E}^{\mathrm{e}} : \boldsymbol{\epsilon}(\boldsymbol{u}) = \mathsf{E}^{\mathrm{e}} : \boldsymbol{H}(\boldsymbol{u}), \tag{3.5}$$

where $\boldsymbol{\epsilon}(\boldsymbol{u}) \stackrel{\text{def}}{=} \boldsymbol{H}(\boldsymbol{u})^{\text{sym}}$ is the (small) strain operator and E^{e} is the constant elastic stiffness tensor. It appears that $\tilde{\boldsymbol{\Sigma}}$ can be computed a posteriori when the solution $\boldsymbol{u}$ to the direct motion problem is available.

Consider now an arbitrary subdomain $A \subset \Omega$ with boundary Γ. From equilibrium (3.2), the resultant to the material tractions along Γ must vanish

$$\int_{\Gamma} \tilde{\boldsymbol{\Sigma}} \cdot \boldsymbol{n} \, \mathrm{d}\Gamma = \mathbf{0}, \tag{3.6}$$

where $\boldsymbol{n}$ is the outward unit normal to Γ. We now consider the case when the boundary is non-smooth such that Γ can be decomposed into a regular part Γ^{r} and a singular part Γ^{s} (comprising a notch, a crack tip, etc.) with $\Gamma = \Gamma^{\mathrm{r}} \cup \Gamma^{\mathrm{s}}$ and $\Gamma^{\mathrm{r}} \cap \Gamma^{\mathrm{s}} = \emptyset$, see Figure 1. We use (3.6) to single out the resultant vector force on the singular part Γ^{s}

$$\boldsymbol{F}_{\text{mat}} \stackrel{\text{def}}{=} -\int_{\Gamma^{\mathrm{s}}} \tilde{\boldsymbol{\Sigma}} \cdot \boldsymbol{n} \, \mathrm{d}\Gamma = \int_{\Gamma^{\mathrm{r}}} \tilde{\boldsymbol{\Sigma}} \cdot \boldsymbol{n} \, \mathrm{d}\Gamma. \tag{3.7}$$

We now define the (generalized) J-integral as the projection of $\boldsymbol{F}_{\text{mat}}$ in the direction of a possible unit extension $\boldsymbol{e}$ of the notch, crack, etc

$$J \stackrel{\text{def}}{==} \boldsymbol{e} \cdot \boldsymbol{F}_{\text{mat}} = \int_{\Gamma^{\mathrm{r}}} \boldsymbol{e} \cdot \tilde{\boldsymbol{\Sigma}} \cdot \boldsymbol{n} \, \mathrm{d}\Gamma. \tag{3.8}$$

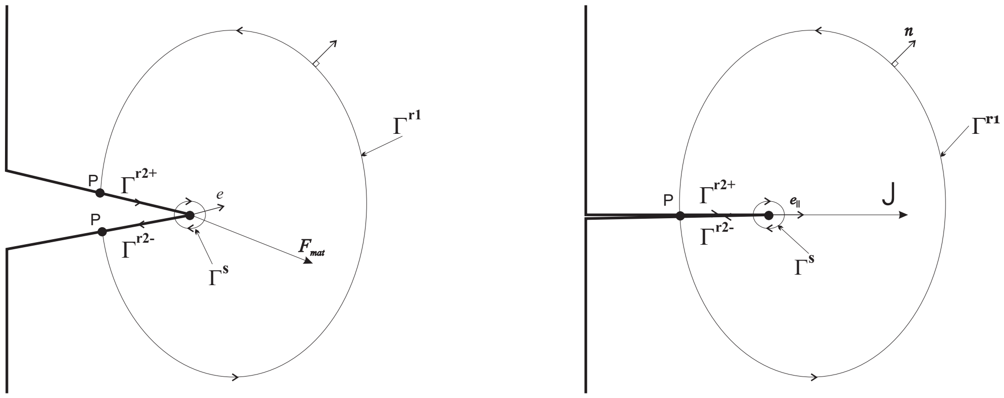

FIGURE 1. Arbitrary subdomain with regular ($\Gamma^{\mathrm{r}} = \Gamma^{\mathrm{r1}} + \Gamma^{\mathrm{r2+}} + \Gamma^{\mathrm{r2-}}$) and singular ($\Gamma^{\mathrm{s}}$) parts. a) Notch with concentrated force acting on singular point and b) straight crack and J-integral.

3.2. **Different formats of the J-integral.** Consider the weak format of (3.2), which can be rewritten as

$$F_{\mathrm{mat}}(\boldsymbol{w}) \stackrel{\mathrm{def}}{=} -\int_{\Gamma^{\mathrm{s}}} \boldsymbol{w} \cdot \tilde{\boldsymbol{\Sigma}} \cdot \boldsymbol{n} \, \mathrm{d}\Gamma = \int_{\Gamma^{\mathrm{r}}} \boldsymbol{w} \cdot \tilde{\boldsymbol{\Sigma}} \cdot \boldsymbol{n} \, \mathrm{d}\Gamma - \int_{A} \boldsymbol{H}(\boldsymbol{w}) : \tilde{\boldsymbol{\Sigma}} \, \mathrm{d}A, \tag{3.9}$$

for all virtual displacements $\boldsymbol{w}(\boldsymbol{x})$ of sufficient regularity. Next, we consider the special case of a straight, traction-free, crack, which is tested for a possible extension in the same direction, see Figure 1.

It is interesting to note that the J-integral in this case can be retrieved from (3.9) in three different ways:

- **Contour integral format**
  Setting $\boldsymbol{w}(\boldsymbol{x}) = \boldsymbol{e}_{||}$ (constant) in (3.9) gives

$$J = F_{\mathrm{mat}}(\boldsymbol{e}_{||}) = \int_{\Gamma^{\mathrm{r}_1}} \boldsymbol{e}_{||} \cdot \tilde{\boldsymbol{\Sigma}} \cdot \boldsymbol{n} \, \mathrm{d}\Gamma, \tag{3.10}$$

  where it was used that $\boldsymbol{H}(\boldsymbol{e}_{||}) = \boldsymbol{0}$ in the subdomain A and that the contribution from the crack faces vanishes (since $\boldsymbol{e}_{||} \cdot \boldsymbol{n} = 0$ and $\boldsymbol{\sigma} \cdot \boldsymbol{n} = \boldsymbol{0}$).
- **Domain integral format**
  Setting $\boldsymbol{w}(\boldsymbol{x}) = q(\boldsymbol{x})\boldsymbol{e}_{||}$ with $q = 1$ on Γ^{s} and letting q decay within the chosen domain until $q = 0$ at Γ^{r_1}, we obtain from (3.9)

$$J \;=\; F_{\mathrm{mat}}(q\boldsymbol{e}_{||}) = -\int_{A} \boldsymbol{H}(q\boldsymbol{e}_{||}) : \tilde{\boldsymbol{\Sigma}} \, \mathrm{d}\Omega = -\int_{A} (\boldsymbol{e}_{||} \otimes \nabla q) : \tilde{\boldsymbol{\Sigma}} \, \mathrm{d}\Omega, \tag{3.11}$$

  where it was used that the boundary integral vanishes on Γ^{r_1} (since $q = 0$). Introducing the material force resultant

$$\boldsymbol{F}_{\mathrm{mat}}(q) \stackrel{\mathrm{def}}{=} -\int_{A} \tilde{\boldsymbol{\Sigma}} \cdot \nabla q \, \mathrm{d}\Omega, \tag{3.12}$$

as a vector functional of the chosen $q(\boldsymbol{x})$ within the chosen domain A yields

$$J = \boldsymbol{e}_{||} \cdot \boldsymbol{F}_{\text{mat}}(q). \tag{3.13}$$

Remark: In practice, $q(\boldsymbol{x}_c) = 1$ at the crack tip $\boldsymbol{x} = \boldsymbol{x}_c$. $\square$

- **Node integral format**
  As a special case of (3.13), due to the possibility to choose the subdomain arbitrary, we consider the limit situation when A shrinks to nothing. Letting A be parametrizised by a typical radius r, we formally obtain

$$J = \lim_{r\to 0} F_{\text{mat}}(q\boldsymbol{e}_{||}) = \lim_{r\to 0} \boldsymbol{e}_{||} \cdot \boldsymbol{F}_{\text{mat}}(q). \tag{3.14}$$

Remark: The notation 'node integral format' alludes to the corresponding finite element approximation, cf. below. $\square$

Further background material on the contour and domain formats for computing J can be found in [7], [8] and [9].

3.3. **Finite element approximation.** In a finite element setting we choose $\boldsymbol{w}(\boldsymbol{x}) \approx \boldsymbol{w}_h(\boldsymbol{x}) = \sum_n N^n(\boldsymbol{x})\boldsymbol{W}^n$, where N^n is the basis function associated with the node at $\boldsymbol{x} = \boldsymbol{x}_n$ and $\boldsymbol{W}^n$ is the nodal displacement vector. Hence, we obtain

$$F_{\text{mat}}(\boldsymbol{w}_h) \;=\; \sum_n \boldsymbol{W}^n \cdot \boldsymbol{F}^n_{\text{mat}}, \tag{3.15}$$

where we introduced

$$\boldsymbol{F}^n_{\text{mat}} \;\stackrel{\text{def}}{=}\; \int_{\Gamma^{\text{r}}_n} N^n \tilde{\boldsymbol{\Sigma}} \cdot \boldsymbol{n}\; \mathrm{d}\Gamma - \int_{A_n} \tilde{\boldsymbol{\Sigma}} \cdot \nabla N^n \; \mathrm{d}\Omega, \tag{3.16}$$

i.e. $\boldsymbol{F}^n_{\text{mat}}$ is the material nodal force (vector) associated with the basis function N^n for $n = 1, 2, 3, .., N$, and where $A_n \subset A$ is the part of A where N^n has support. Moreover, Γ_n is the boundary of A_n and in order to account for singularities we decompose Γ_n as $\Gamma_n = \Gamma^{\text{r1}}_n \cup \Gamma^{\text{r2+}}_n \cup \Gamma^{\text{r2}-}_n \cup \Gamma^{\text{s}}_n$. Expanding $q(\boldsymbol{x}) = \sum_n N^n(\boldsymbol{x}) Q_n$, we may thus summarize:

- **Domain integral format**

$$J_h(\boldsymbol{u}) = -\sum_n Q_n \int_{A_n} (\boldsymbol{e}_{||} \otimes \boldsymbol{\nabla} N^n) : \tilde{\boldsymbol{\Sigma}}(\boldsymbol{u})\; \mathrm{d}\Omega. \tag{3.17}$$

- **Node integral format**

$$J_h(\boldsymbol{u}) = -\int_{A_{n_c}} (\boldsymbol{e}_{||} \otimes \boldsymbol{\nabla} N^{n_c}) : \tilde{\boldsymbol{\Sigma}}(\boldsymbol{u})\; \mathrm{d}\Omega. \tag{3.18}$$

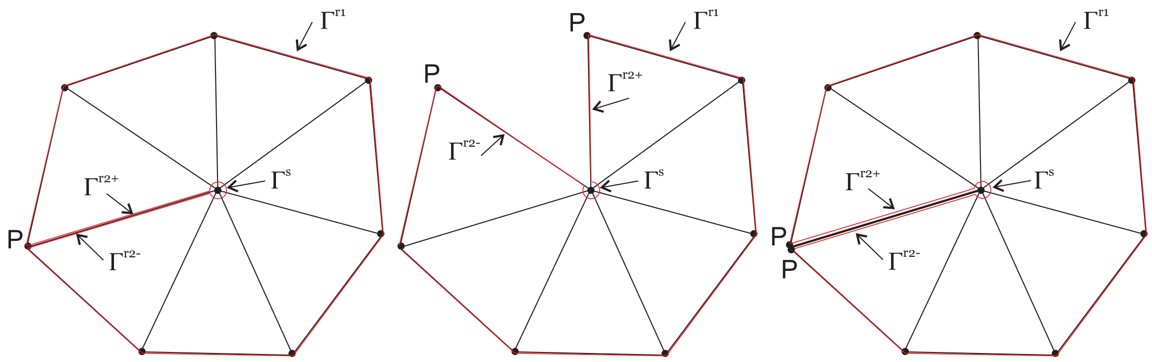

FIGURE 2. Three different situations: a) internal node, b) external node and c) crack tip node.

3.4. **The internal, external(notch) and crack tip node.** Consider the three different situations schematically described in Figure 2.

- **Internal node**
  In this case $N^n = 0$ on Γ_n^{r1}. Moreover, the contributions from $\Gamma_n^{\text{r2}+}$ and $\Gamma_n^{\text{r2}-}$ are (in the continuous formulation) self-equilibrating. This yields

$$\boldsymbol{F}_{\text{mat}}^n = -\int_{A_n} \tilde{\boldsymbol{\Sigma}} \cdot \nabla N^n \, d\Omega. \tag{3.19}$$

  In the discrete setting there are jumps in the tractions along Γ_n^{r2}, hence, the contribution is in general not self-equilibrating. For a sufficient resolution, however, the contribution is small and could be neglected without loss of accuracy.

- **External (Notch) node**
  In this case $N^n = 0$ on Γ_n^{r1}, whereas $N^n \neq 0$ on $\Gamma_n^{\text{r2}+} \cup \Gamma_n^{\text{r2}-}$. Hence, the contribution from the surface integral does not vanish and we have

$$\boldsymbol{F}_{\text{mat}}^n = \int_{\Gamma_n^{\text{r2}}} N^n \tilde{\boldsymbol{\Sigma}} \cdot \boldsymbol{n} \, d\Gamma - \int_{A_n} \tilde{\boldsymbol{\Sigma}} \cdot \nabla N^n \, d\Omega \tag{3.20}$$

  In case there are no physical tractions along $\Gamma_n^{\text{r2}+} \cup \Gamma_n^{\text{r2}-}$ we have $\tilde{\Sigma} \cdot \boldsymbol{n} = W\boldsymbol{n}$ and the material tractions will not vanish.

- **Crack tip node**
  A special case, the notch degenerates into a crack with parallel surfaces. Further, in the case that we want to compute the J-integral of a straight, traction free crack for a possible straight extension, then $\boldsymbol{e}_{||} \cdot \boldsymbol{n} = 0$ and the contribution from Γ_n^{r2} vanishes. Hence, (3.20) becomes

$$\boldsymbol{F}_{\text{mat}}^n = -\int_{A_n} \tilde{\boldsymbol{\Sigma}} \cdot \nabla N^n \, d\Omega \tag{3.21}$$

  For $n = n_c$, defining the crack tip node, we may compute the FE-discretized $J \approx J_h$ from the domain or node integral format by setting $n = n_c$ in (3.21).

4. Goal quantities and their linearization

4.1. **Contour integral format.** Choosing the contour integral format for computing J leads to

$$Q(\boldsymbol{u}) = \int_\Gamma \boldsymbol{e}_{||} \cdot \tilde{\boldsymbol{\Sigma}}(\boldsymbol{u}) \cdot \boldsymbol{n} \, \mathrm{d}\Gamma, \tag{4.1}$$

with the associated linearization

$$E'(\boldsymbol{u}, \boldsymbol{u}_h; \boldsymbol{w}) = \int_\Gamma \left(\boldsymbol{e}_{||} \otimes \boldsymbol{n}\right) : \tilde{\mathsf{C}} : \boldsymbol{H}(\boldsymbol{w}) \, \mathrm{d}\Gamma, \tag{4.2}$$

where $\tilde{\mathsf{C}}$ is the tangent stiffness tensor associated with the Newton-Eshelby material stress $\tilde{\boldsymbol{\Sigma}}$ with respect to a variation of the (physical) strain field:

$$\tilde{\mathsf{C}} = \boldsymbol{I} \otimes \boldsymbol{\sigma} - \boldsymbol{I} \underline{\otimes} \boldsymbol{\sigma} - \boldsymbol{H}^T \cdot \mathsf{E}^{\mathrm{e}}. \tag{4.3}$$

In practice, we linearize $\tilde{\mathsf{C}}$ using a p-refined approximation for $\boldsymbol{u}$.

The contour Γ can, without restriction on the theoretical applicability, be chosen as a path of element edges (defining the boundary of A) in the finite element subdivision of Ω.

4.2. **Domain integral format.** Choosing the domain integral format for computing J leads to

$$Q(\boldsymbol{u}) = -\int_A \left(\boldsymbol{e}_{||} \otimes \boldsymbol{\nabla} q\right) : \tilde{\boldsymbol{\Sigma}}(\boldsymbol{u}) \, \mathrm{d}\Omega, \tag{4.4}$$

with the associated linearization

$$E'(\boldsymbol{u}, \boldsymbol{u}_h; \boldsymbol{w}) = -\int_A \left(\boldsymbol{e}_{||} \otimes \boldsymbol{\nabla} q\right) : \tilde{\mathsf{C}}(\bar{\boldsymbol{u}}) : \boldsymbol{H}(\boldsymbol{w}) \, \mathrm{d}A. \tag{4.5}$$

In the finite element approximation of $Q(\boldsymbol{u}) = J_h(\boldsymbol{u}) \approx J_h(\boldsymbol{u}_h)$, the expression (3.17) is used.

4.3. **Node integral format.** Choosing the node integral format for computing J leads to (in practice)

$$Q(\boldsymbol{u}) = -\lim_{r \to 0} \int_{A_{n_c}} \left(\boldsymbol{e}_{||} \otimes \boldsymbol{\nabla} N^{n_c}\right) : \tilde{\boldsymbol{\Sigma}}(\boldsymbol{u}) \, \mathrm{d}\Omega, \tag{4.6}$$

where r is a typical diameter of A_{n_c}. The associated linearization obviously becomes

$$E'(\boldsymbol{u}, \boldsymbol{u}_h; \boldsymbol{w}) = -\lim_{r \to 0} \int_{A_{n_c}} \left(\boldsymbol{e}_{||} \otimes \boldsymbol{\nabla} N^{n_c}\right) : \tilde{\mathsf{C}}(\bar{\boldsymbol{u}}) : \boldsymbol{H}(\boldsymbol{w}) \, \mathrm{d}A. \tag{4.7}$$

In the finite element approximation $Q(\boldsymbol{u}) = J_h(\boldsymbol{u}) \approx J_h(\boldsymbol{u}_h)$, the expression in (3.18) is used.

Remark: At any 'regular' node, the associated material force $\boldsymbol{F}^n_{\mathrm{mat}}$ should vanish at sufficient mesh refinement, i.e.,

$$\lim_{h \to 0} \boldsymbol{e}_{||} \cdot \boldsymbol{F}^n_{\mathrm{mat}} = \begin{pmatrix} J & \text{when} & n = n_c \\ 0 & \text{when} & n \neq n_c \end{pmatrix}. \tag{4.8}$$

Hence, it would be possible to define a global measure Q that accounts for this fact. For example, choosing $A = \Omega$ and $\boldsymbol{w} = \boldsymbol{u}$ (the exact solution), we expect to obtain $F_{\text{mat}}(\boldsymbol{u}) = \boldsymbol{u}(\boldsymbol{x_c}) \cdot \boldsymbol{F}_{\text{mat}}$. At least, the values $\boldsymbol{F}^n_{\text{mat}}$ should give information that can be used to move the nodes and improve the quality of the mesh. Indeed, such a strategy was recently suggested by Mueller et al. [10]. □

5. A comparison between the integral formats for computing J

Consider the pre-cracked plate in Figure 3 with the dimension w = 0.5m, h = 1.0m, and crack length a = 0.1m. The plate is loaded along its upper boundary by the traction $\boldsymbol{t} = [0, 1\text{e}{+}06]^T$N. The elasticity parameters are E = 210e+09Pa and $\nu = 0.3$.

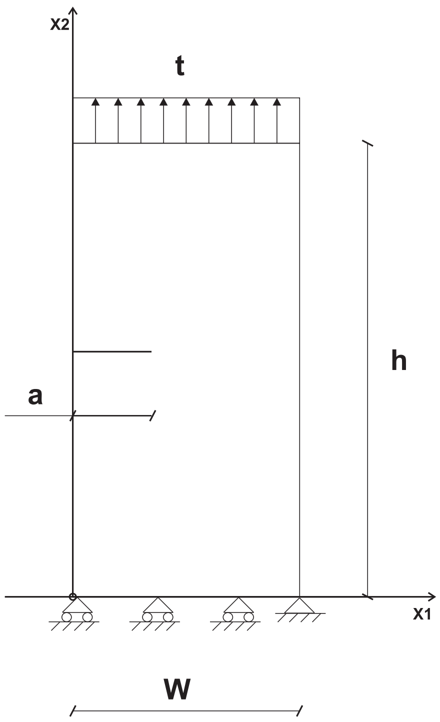

Figure 3. Plate with a single-edged crack of length a.

Figure 4 shows how the different methods used for computing J result in different adapted grids to meet the required tolerance $TOL = 0.5\%$. Figures 5-6 show the convergence rate and the effectivity index η, respectively. In these figures we use the notation

$$\bar{h} = \frac{\mathrm{m}(\Omega)}{\sqrt{N^{el}}}, \qquad \eta = \frac{F(\tilde{\boldsymbol{\varphi}} - \boldsymbol{\pi}_h\tilde{\boldsymbol{\varphi}}) - a(\boldsymbol{u}_h; \tilde{\boldsymbol{\varphi}} - \boldsymbol{\pi}_h\tilde{\boldsymbol{\varphi}})}{Q(\boldsymbol{u}) - Q(\boldsymbol{u}_h)}, \tag{5.1}$$

where N^{el} is the number of elements in the mesh. The improved dual solution $\tilde{\boldsymbol{\varphi}}$ is computed with quadratic approximation. In Figure 5 we can see that the convergence rate is much higher for the contour and domain integral methods. The reason for this is that linear elements do not capture the $\frac{1}{\sqrt{r}}$ singularity very well. The plot in Figure 6 shows that the error representation formula for the node integral method gives an error estimate approximately 40% below the actual error, which should be compared with $10-20\%$ for the other considered methods.

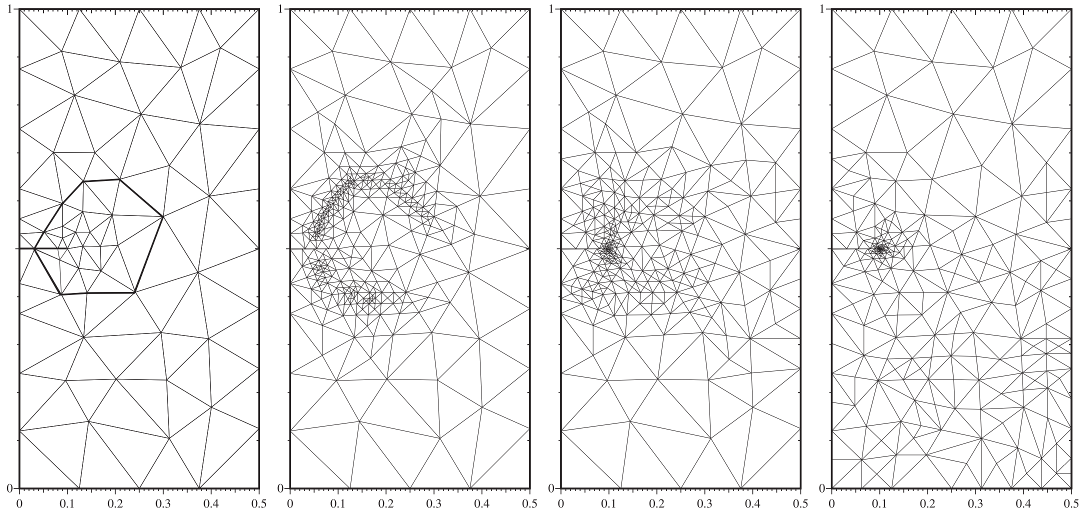

FIGURE 4. Adaptive meshes for the different methods used to compute J. From left: initial mesh and contour Γ, contour integral method, domain integral method and, finally, node integral method.

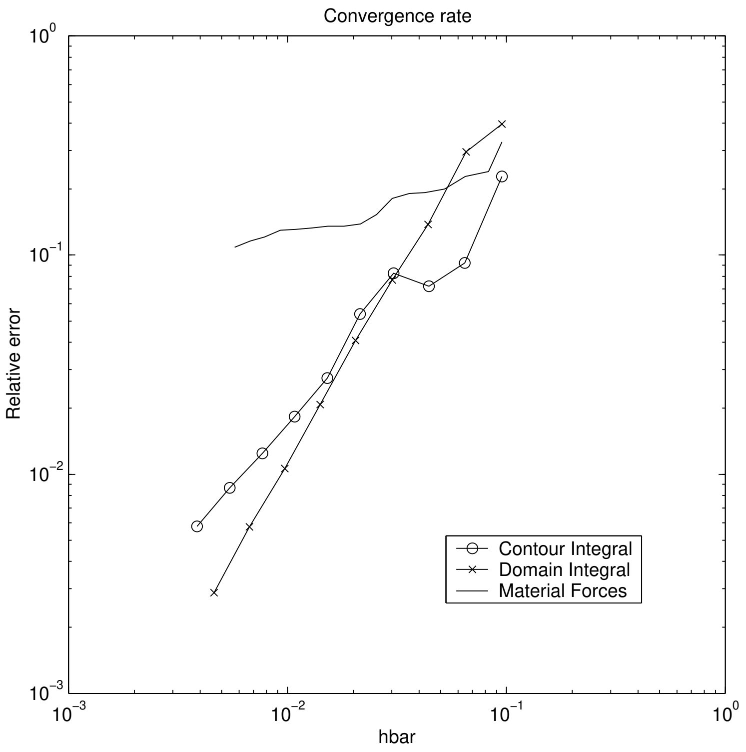

FIGURE 5. Convergence rate for different methods to compute J.

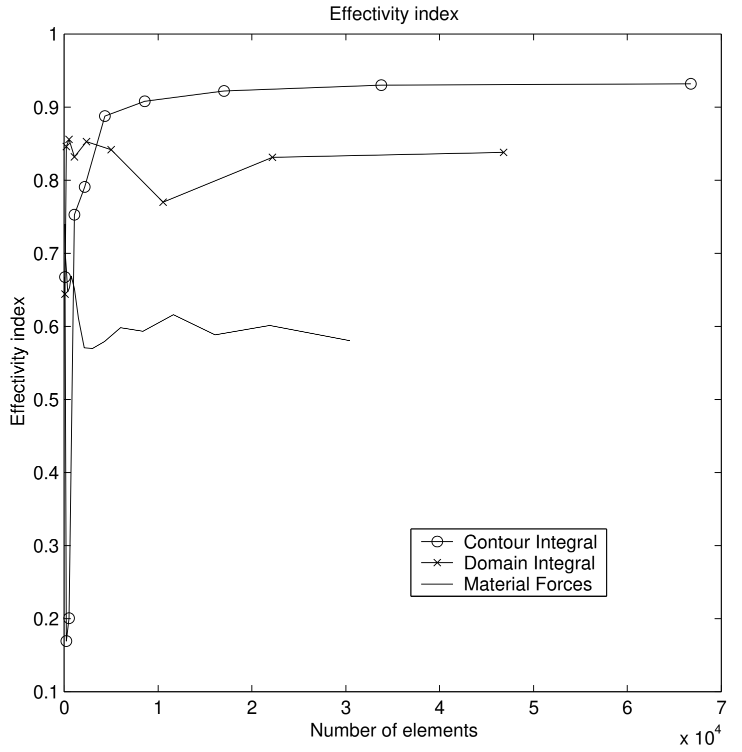

FIGURE 6. Effectivity index for different methods to compute J.

5.1. **Edge notch.** We now concider the case when the crack edges are not parallel such that the contribution from Γ^{r2} is not zero.

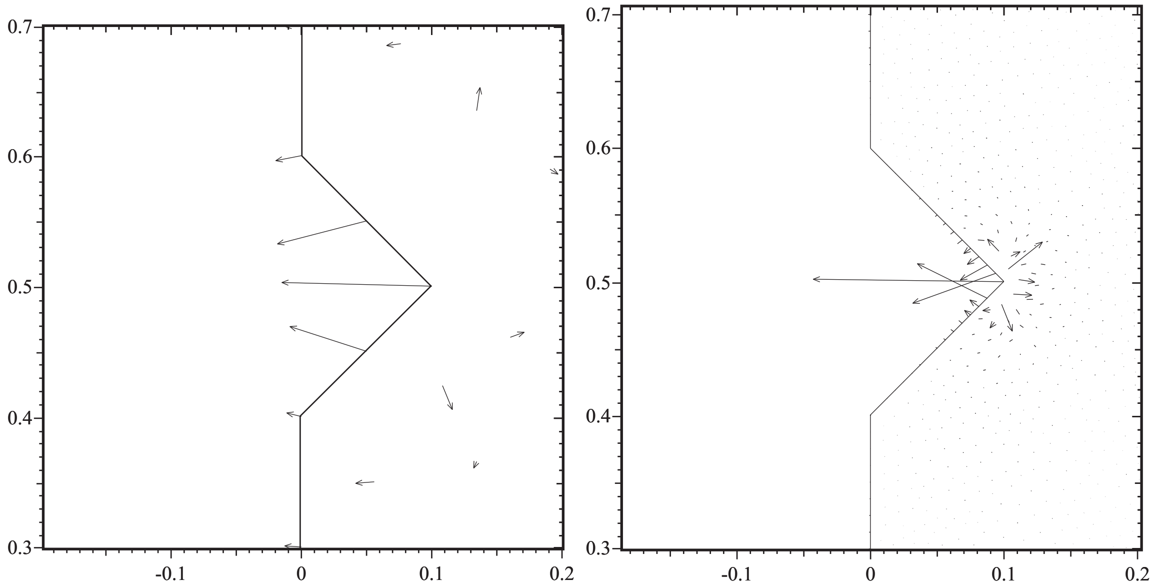

FIGURE 7. The discrete material force vectors acting on the nodes. a) Coarse mesh and large material forces along the notch boundary and b) fine mesh and more localized boundary effect.

In Figure 7 we show the resulting discrete nodal material force vectors obtained for two different meshes. As expected, the internal and external forces decrease for a refined mesh. The large forces acting around the crack tip node are due to the inability to resolve the singularity with ordinary elements. In this figure we use linear approximation, i.e. piecewise constant stresses. An asymptotic study of the contribution from the boundary term, for a sequence of refined grids is shown in Figure 8. For a typical non-singular node on the boundary the material forces vanish for a sufficiently refined mesh. However, for a singular (crack tip) node the contribution is still about 1%. This shows that the boundary term can not be neglected when computing the material force vector for a singular node.

5.2. **Summary and outlook.** We have recalled the theory for goal-oriented adaptivity together with an introduction to the 'material force' concept. An adaptive strategy was applied to the fracture mechanics problem of a straight traction free crack, whereby different methods to compute the energy release rate were compared. The results show that the contour and domain integral formulations yield the best results in terms of convergence rates and effectivity index. It was also noticed that the contribution from the crack faces cannot be neglected in case the crack edges are not perpendicular to the anticipated direction of crack extension. Future development would include the incorporation of a fictitious crack with the appropriate cohesive law. Moreover, curved cracks and closed cracks with friction, where the boundary term also includes the physical tractions, should be studied.

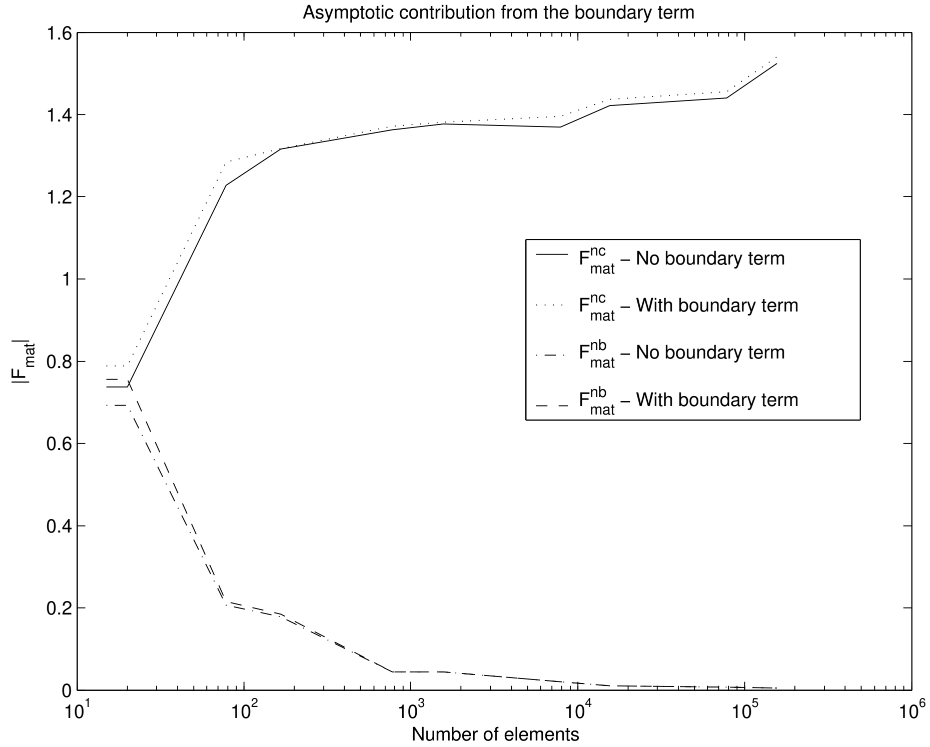

FIGURE 8. This plot shows the contribution from the boundary term. The length of the material force vector vs the of number of elements. We use the superscript *nc* for the singular (crack tip) node and *nb* for a regular (boundary) node

REFERENCES

[1] P. Steinmann. Application of Material Forces to Hyperelastostatic Fracture Mechanics. Part I: Continuum mechanical setting. *International Journal of Solids and Structures* 2000; **37**:7371–7391.

[2] P. Steinmann, D. Ackermann, F. J. Barth, Application of Material Forces to Hyperelastostatic Fracture Mechanics. Part II: Computational setting. *International Journal of Solids and Structures* 2001; **38**:5509–5526.

[3] K. Eriksson, D. Estep, P. Hansbo, C. Johnson. Introduction to adaptive methods for differential equations. *Acta Numerica* 1995; 105-108.

[4] R. Becker, R. Rannacher. A feed-back approach to error control in finite element methods: basic analysis and examples. *East-West Journal of Numerical Mathematics* 1996; **4**:237-264.

[5] F. Larsson, P. Hansbo, K. Runesson. Strategies for computing goal-oriented a posteriori error measures in non-linear elasticity. *International Journal for Numerical Methods in Engineering* 2002; **55**:879-874.

[6] M. Rüter, E. Stein, *Goal-Oriented A Posteriori Error Estimates in Elastic Fracture Mechanics*, Proceedings of the Fifth World Congress on Computational Mechanics (WCCM V), July 7-12, 2002, Vienna, Austria, Editors: Mang, H.A; Rammerstorfer, F.G; Eberhardsteiner, J., Publisher: Vienna University of Technology, Austria, ISBN 3-9501554-0-6, http://wccm.tuwien.ac.at

[7] J.R Rice. A path independent integral and the approximate analysis of strain concentration by notches and cracks. *Journal of Applied Mechanics* 1968; **35**:379–386.

[8] F.Z. Li, C.F. Shih, A. Needleman. A comparison of methods for calculating energy release rates. *Engineering Fracture Mechanics* 1985; **21**:405-421.
[9] C.F. Shih, B. Moran, T. Nakamura. Energy release rate along a three-dimensional crack front in a thermally stressed body. *International Journal of Fracture* 1986; **30**:79-102.
[10] R. Mueller, S. Kolling, D. Gross, On configurational forces in the context of the finite element method. *International Journal for Numerical Methods in Engineering* 2002; **53**:1557–1574.

Chalmers Finite Element Center Preprints

2001–01 *A simple nonconforming bilinear element for the elasticity problem*
Peter Hansbo and Mats G. Larson

2001–02 *The $\mathcal{LL}^*$ finite element method and multigrid for the magnetostatic problem*
Rickard Bergström, Mats G. Larson, and Klas Samuelsson

2001–03 *The Fokker-Planck operator as an asymptotic limit in anisotropic media*
Mohammad Asadzadeh

2001–04 *A posteriori error estimation of functionals in elliptic problems: experiments*
Mats G. Larson and A. Jonas Niklasson

2001–05 *A note on energy conservation for Hamiltonian systems using continuous time finite elements*
Peter Hansbo

2001–06 *Stationary level set method for modelling sharp interfaces in groundwater flow*
Nahidh Sharif and Nils-Erik Wiberg

2001–07 *Integration methods for the calculation of the magnetostatic field due to coils*
Marzia Fontana

2001–08 *Adaptive finite element computation of 3D magnetostatic problems in potential formulation*
Marzia Fontana

2001–09 *Multi-adaptive galerkin methods for ODEs I: theory & algorithms*
Anders Logg

2001–10 *Multi-adaptive galerkin methods for ODEs II: applications*
Anders Logg

2001–11 *Energy norm a posteriori error estimation for discontinuous Galerkin methods*
Roland Becker, Peter Hansbo, and Mats G. Larson

2001–12 *Analysis of a family of discontinuous Galerkin methods for elliptic problems: the one dimensional case*
Mats G. Larson and A. Jonas Niklasson

2001–13 *Analysis of a nonsymmetric discontinuous Galerkin method for elliptic problems: stability and energy error estimates*
Mats G. Larson and A. Jonas Niklasson

2001–14 *A hybrid method for the wave equation*
Larisa Beilina, Klas Samuelsson and Krister Åhlander

2001–15 *A finite element method for domain decomposition with non-matching grids*
Roland Becker, Peter Hansbo and Rolf Stenberg

2001–16 *Application of stable FEM-FDTD hybrid to scattering problems*
Thomas Rylander and Anders Bondeson

2001–17 *Eddy current computations using adaptive grids and edge elements*
Y. Q. Liu, A. Bondeson, R. Bergström, C. Johnson, M. G. Larson, and K. Samuelsson

2001–18 *Adaptive finite element methods for incompressible fluid flow*
Johan Hoffman and Claes Johnson

2001–19 *Dynamic subgrid modeling for time dependent convection–diffusion–reaction equations with fractal solutions*
Johan Hoffman

2001–20 *Topics in adaptive computational methods for differential equations*
Claes Johnson, Johan Hoffman and Anders Logg

2001–21 *An unfitted finite element method for elliptic interface problems*
Anita Hansbo and Peter Hansbo

2001–22 *A P^2–continuous, P^1–discontinuous finite element method for the Mindlin-Reissner plate model*
Peter Hansbo and Mats G. Larson

2002–01 *Approximation of time derivatives for parabolic equations in Banach space: constant time steps*
Yubin Yan

2002–02 *Approximation of time derivatives for parabolic equations in Banach space: variable time steps*
Yubin Yan

2002–03 *Stability of explicit-implicit hybrid time-stepping schemes for Maxwell's equations*
Thomas Rylander and Anders Bondeson

2002–04 *A computational study of transition to turbulence in shear flow*
Johan Hoffman and Claes Johnson

2002–05 *Adaptive hybrid FEM/FDM methods for inverse scattering problems*
Larisa Beilina

2002–06 *DOLFIN - Dynamic Object oriented Library for FINite element computation*
Johan Hoffman and Anders Logg

2002–07 *Explicit time-stepping for stiff ODEs*
Kenneth Eriksson, Claes Johnson and Anders Logg

2002–08 *Adaptive finite element methods for turbulent flow*
Johan Hoffman

2002–09 *Adaptive multiscale computational modeling of complex incompressible fluid flow*
Johan Hoffman and Claes Johnson

2002–10 *Least-squares finite element method with applications in electromagnetics*
Rickard Bergström

2002–11 *Discontinuous/continuous least-squares finite element methods for Elliptic Problems*
Rickard Bergström and Mats G. Larson

2002–12 *Discontinuous least-squares finite element methods for the Div-Curl problem*
Rickard Bergström and Mats G. Larson

2002–13 *Object oriented implementation of a general finite element code*
Rickard Bergström

2002-14 *On adaptive strategies and error control in fracture mechanics*
Per Heintz and Klas Samuelsson

2002-15 *A unified stabilized method for Stokes' and Darcy's equations*
Erik Burman and Peter Hansbo

2002-16 *A finite element method on composite grids based on Nitsche's method*
Anita Hansbo, Peter Hansbo and Mats G. Larson

2002-17 *Edge stabilization for Galerkin approximations of convection–diffusion problems*
Erik Burman and Peter Hansbo

2002-18 *Adaptive strategies and error control for computing material forces in fracture mechanics.*
Per Heintz, Fredrik Larsson, Peter Hansbo and Kenneth Runesson

These preprints can be obtained from

`www.phi.chalmers.se/preprints`